SPACE CHARGE

Space charges literally mean charges in space, that is, in a region where there is a concentration of charges and/or ions of one polarity. These charges may be mobile electrons, holes, or localized ionized impurities. The space charge density ρ is given by

$$\rho = Ne \tag{1}$$

where N is the total number of charges and e the electronic charge. In insulating and semiconducting materials,

$$N = p - n + N_{\mathrm{d}}^{+} - N_{\mathrm{a}}^{-} \tag{2}$$

. . . where p and n are the free hole and electron densities, respectively, and N_{d}^{+} and N_{a}^{+} denote the densities of localized and ionized donor and acceptor centers. Equations (1) and (2) are valid for all insulating and semiconducting materials, even in the presence of nonequilibrium charge densities. In a region where there is a concentration of charges and/or ions of one polarity the electrostatic field will be distorted.

A passage of these charges in the presence of an electric field will constitute a current. Space-charge currents have been observed in many materials including vacuum, insulating organic solids and liquids, and inorganic semiconductors. Many electronic devices, namely, vacuum tubes, p–n junctions, Gunn diodes, electrets, and so on exploit the phenomenon of space-charge formation. It is equally true that serious structural degradation and aging may occur in electrical insulating materials due to charge injection, leading to the formation of space charges and subsequent electrical breakdown. In insulating organic solids the concept of a critical electric field level above which fast charge carrier transport occurs has been developed by Zeller and Schneider (1). It has also been suggested that charges trapped in the bulk of an insulating organic polymer play an important part in the initiation and propagation of ionization waves and a transition to a local breakdown may originate from the space-charge neutralization process and its dynamics (2). The nature of a metal–polymer interface plays a crucial role for the injection of excess charges in the presence of an external field, and the space-charge distribution in the polymer will depend on its morphology and the mobility of the charge carriers. For example, a high concentration of localized charges may be expected at the crystalline–amorphous interface, around morphological defects, around inclusions, and around impurities in semicrystalline and chemically cross-linked polyethylene. A concentration of localized states will modify the local field, obeying Poisson's equation [see Eq. (3)]. At very high fields ($\geq 10^9$ $\mathrm{V \cdot m^{-1}}$) the space charges will acquire high mobility (1), thus reducing the concentration. Hence an upper limit to the space-charge concentration is provided by the field-dependent charge mobility (3).

In general, the performance of high-voltage (HV) cables is significantly and adversely affected by the development of the space-charge distribution, which affects electrical conduction and breakdown phenomena. Space-charge evolution near the electrodes has also been observed in dilute binary electrolytes exposed to HV transients (4). Charge-injection processes with electrodes immersed in dielectric liquids with low permittivities are well known (5). Space-charge electrets are useful devices that can store real charges quasipermanently in the bulk and also at the surface, and these devices have diverse applications such as electret microphones, radiation dosimeters, and gas filters. Recently, a review was presented on space-charge electrets (6), which also surveyed their possible new applications.

Measurements of space charges in insulating materials can be made by the conventional technique of conduction current measurement and thermally stimulated discharge current (TSDC) studies. The latter method provides no information on the spatial distribution of space charges. However, since 1980, there have been several useful experimental methods, both nondestructive and destructive, that measure the spatial distribution of polarization and charges with a resolution of approximately 1 μm in the thickness direction (7,8). These quantitative measurement techniques of space charges and their spatial distribution will be reviewed in this article.

SPACE-CHARGE-LIMITED CURRENT

Langmuir derived the theoretical relation between the voltage applied to a pair of electrodes and the resulting electron current in a high vacuum. However, the same equation was previously derived by Child for the case of a current due to positive ions in arcs at low pressure. Macroscopically, Poisson's equation, which holds for any point in space where a space-charge density ρ exists, expresses excess charge in one dimension as

$$\frac{d^2V}{dx^2} = -\frac{\rho}{\epsilon_0 \epsilon_{\mathrm{r}}} \tag{3}$$

where ϵ_0 is the vacuum permittivity and ϵ_{r} the relative permittivity of the dielectric material. ρ is given by

$$\rho = \frac{J}{(2eV/m)^{1/2}} \tag{4}$$

where J is the current density and e and m are the electronic charge and mass, respectively. Substituting Eq. (4) in Eq. (3) and solving V, it may be shown that (9)

$$J = \frac{4}{9x^2}\epsilon_0 \left(\frac{2e}{m}\right)^{1/2} V^{3/2} \tag{5}$$

for the vacuum case. Equation (5) is the well-known Child–Langmuir 3/2-power law for the space-charge-limited current (SCLC) in vacuum. It is not applicable when the current density reaches the temperature-limited emission case at which the space charge is no longer dense enough to screen the electric field from the cathode.

It may be shown that the space-charge-limited current in solids with single carrier injection and no traps is given by Refs. 10 to 13.

$$J = \tfrac{9}{8}\epsilon_0 \epsilon_{\mathrm{r}} \mu \frac{V^2}{L^3} \tag{6}$$

where μ is the charge mobility and L the sample thickness. Equation (6) is known as the Mott and Gurney law for solids

if the current is space charge limited or as Child's law for solids.

For space-charge-limited current with shallow traps and single carrier injection we have (10–13)

$$J = \tfrac{9}{8}\theta\epsilon_0\epsilon_r\mu\frac{V^2}{L^3} \tag{7}$$

where θ is the ratio of free to trapped charge [i.e., $\theta = n(x)/n_t(x)$] and is a constant. Obviously, the smaller the value of θ, the more efficient the traps to localize the injected charge carrier.

Figure 1 shows the complete current–voltage characteristics for a single set of shallow traps that consist of four discrete regions (11). The injected charge carrier density at low voltages is less than the free-carrier density and the current–voltage behavior is ohmic (region 1). When the injected carrier density exceeds that of the free carrier, the current becomes space-charge-limited modified by the traps (region 2). When the traps are full that is, at the voltage trap-filled limit (VTFL), the current rises sharply (region 3) until it reaches the trap-free SCLC value (region 4).

The space-charge-limited current may thus be identified from a study of steady-state conduction current measurement or a function of an externally impressed electric field in which the $\ln J/\ln V$ behavior is represented by Fig. 1 (11).

THE THERMALLY STIMULATED DISCHARGE CURRENT TECHNIQUE

The technique of thermally stimulated discharge current (TSDC) measurements can provide quantitative information of impurity concentrations, of trapped space charges, and of the nature of molecular motion and their local environments including anisotropy in microstructure (14,15). The technique involves heating a dielectric slowly at a constant rate (i.e., 1°C to 4°C/minute) with its electrodes shorted through an electrometer and monitoring the charge release as a current as a function of temperature in the external circuit.

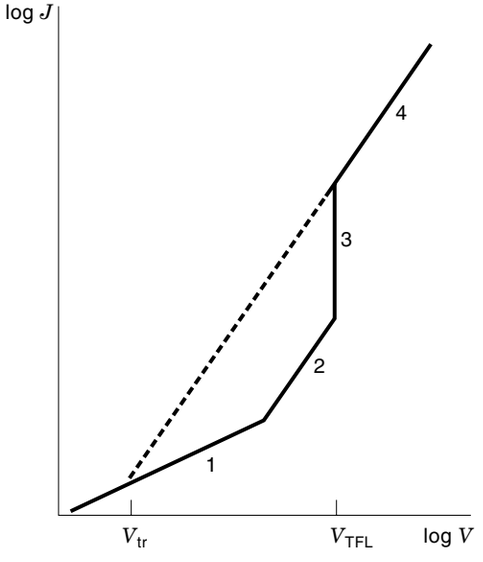

Figure 1. One-carrier space-charge-limited current–voltage characteristic for an insulator with a single trap level. (1) Ohm's law. (2) Modified Mott and Gurney law due to the traps. (3) Trap-filled-limit region. (4) Trap-free Mott and Gurney law (Ref. 11).

These current–temperature spectra may exhibit peaks that can provide information on the trapped space-charge concentration, the charge capture cross section and trap energies, the dipole density, and the dipolar relaxation times.

For a dipolar molecular relaxation process in a TSDC experiment, with the external field $E = 0$, the discharge current $I(t)$ is

$$I(t) = -dP(t)/dt = \alpha P(t) \tag{8}$$

where $P(t)$ is the dielectric polarization as a function of time, $\alpha = 1/\tau(T)$, τ is the relaxation time and T is the temperature. From Eq. (8) we get,

$$P(t) = P_0 \exp\left(-\int_0^t \alpha\, dt\right) \tag{9}$$

where P_0 is the polarization at $t = 0$. Combining Eqs. (8) and (9) and changing the integration from time to temperature using the chain rule, we get

$$I(T) = -\alpha P_0 \exp\left(-b\int_0^T \alpha\, dT\right) \tag{10}$$

where the inverse heating rate b is

$$b = dt/dT \tag{11}$$

Hence $I(T)$ depends on both the inverse of the heating rate b^{-1} and the relaxation frequency. It may be shown that for polymers, with WLF type relaxation processes,

$$I(T) = C_1 \exp\left[-\frac{A}{kT} - \frac{C_2(kT)^2}{A^2}\exp\left(-\frac{A}{kT}\right)\right] \tag{12}$$

where C_1 and C_2 are two adjustable parameters. Equation (12) faithfully reproduces experimentally observed both the TSDC and the thermoluminescence data. A is the activation energy and k Boltzmann's constant.

Persistent electrical polarization can also be developed in solid polymers by direct injection of charges, exposure to electrical coronas, and implantation of ionic species. Excess charges become mobile in the field direction and tend to accumulate in the vicinity of the electrodes to form space-charge polarization. A characteristic peak attributable to a release of space charge, observed in the TSDC spectrum, occurs, in general, at a higher temperature than that for a dipolar orientation, as the latter process only requires a rotation of molecular groups, while the former requires a motion of molecules over a macroscopic distance.

The mathematical analysis of a TSDC spectrum arising from a space-charge contribution can be quite complex. Space charges are dependent on both time and space and involve solutions of nonlinear differential equations that can only be solved analytically for simple charge distributions. It remains a major challenge to establish unequivocally the nature and origin of space-charge peaks and the information derivable from such peaks in TSDC spectra.

DETERMINATION OF SPATIAL DISTRIBUTION OF SPACE CHARGES IN DIELECTRIC MATERIALS

General Information

A knowledge of the spatial distribution of charges in a dielectric is useful in the production and stability of electrets, which are materials with quasipermanent polarization, arising from dipoles and space charges. There are several nondestructive and destructive high-resolution techniques for the determination of spatial charge, polarization, and field profiles. These methods employ, in general, either a nonuniformly distributed thermal force or a mechanical force that interacts with the spatially distributed polarization or space charge to produce pyroelectric or piezoelectric responses, respectively. In addition, there are also photoconductive and spectroscopic methods to determine space-charge distribution in insulators. All these techniques will be discussed in the following sections.

Thermal or Heat Pulse Method (17–24)

In the time domain , the thermal pulse technique may be employed for the determination of spatial distribution of either charges or dipolar polarization in electrets. Dipolar electrets, which exhibit piezo- and pyroelectric properties, are metallized on both sides, whereas the space-charge electrets may be metallized on one side only. Thus for the thermal pulsing experiment different experimental configurations are employed for the dipolar and space-charge electrets (see Fig. 2, Ref. 22). In both configurations nonuniform changes in charge density and polarization are produced by introducing a nonuniform temperature distribution through the respective electrets. These changes, however, are proportional to geometrical changes. For both configurations, the metal electrodes on the front faces are heated by a short light pulse from a gas discharge tube. The method is nondestructive as the temperature change produced by the heat pulse is very small and no permanent changes in the electret occurs. For the case with two metallized electrodes, electrical contacts are made directly to both electrodes and the signal generated by the thermal pulse is fed directly to an amplifier. Both electrodes may be at the same or different potentials initially, the latter condition being introduced by an application of an external voltage. For the single metallized electrode case, the nonmetallized rear surface of the electret is located parallel and close to a guarded electrode, separated by an air gap of about 75 μm. The zero-field condition needs to be maintained for this case, and this is achieved by applying an adjustable external voltage using the well-known Kelvin technique in which the voltage is adjusted to a zero value while the sample is vibrated. Both configurations of the electret can be represented by an equivalent circuit (Fig. 2), containing a capacitive source that provides a signal when the temperature of the electret changes.

In the thermal pulsing technique the heat is absorbed by the thin metallized front electrode surface ($x = 0$) from a very short duration pulse and a voltage change $\Delta V(t)$ is produced across the sample thickness as the heat diffuses to the back ($x = d$) of the electret as a function of time. This voltage change $\Delta V(t)$ is a measure of the charge and polarization distributions and is related to the temperature change $\Delta T(x, t)$. It may be shown that (18)

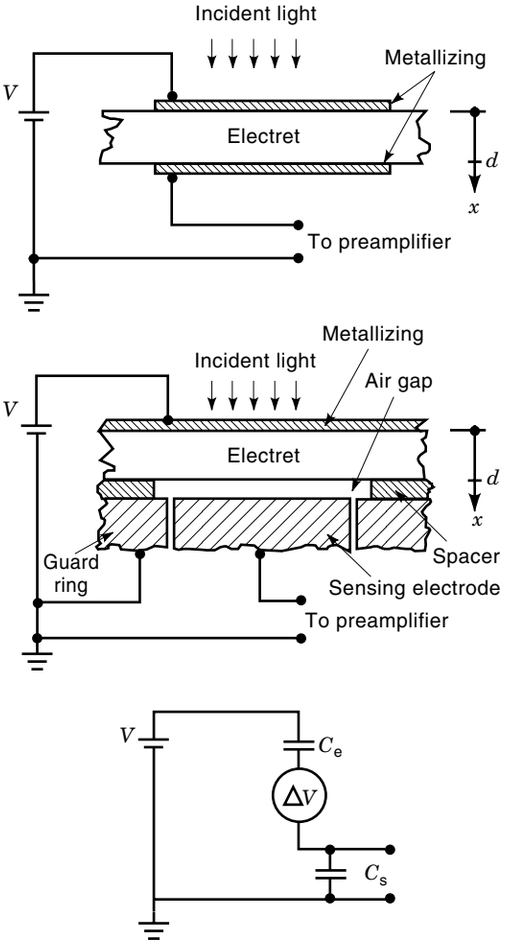

Figure 2. Schematic diagram of the apparatus for the thermal pulsing experiment in the double metallizing and single metallizing configurations. The electrical equivalent circuit of the electret is also shown (Ref. 22).

$$\Delta V(t) = \frac{1}{\epsilon\epsilon_0}\int_0^d \left[\left(A\rho(x) - B\frac{dP}{dx}\right)x\int_0^x \Delta T(x',t)\,dx'\right]dx \quad (13)$$

where $\rho(x)$ and $P(x)$ are the internal charge and polarization distributions, respectively, and

$$\begin{aligned} A &= \alpha_x - \alpha_\epsilon \\ B &= \alpha_p + \alpha_x - \alpha_\epsilon \end{aligned} \quad (14)$$

where α_x, α_ϵ, and α_p are the coefficient of thermal expansion and the temperature coefficients of the dielectric constant ϵ, and the permanent polarization P. For a nonpolar electret, $P = 0$ and we have

$$\Delta V(t) = \frac{\alpha_x - \alpha_\epsilon}{\epsilon\epsilon_0}\int_0^d \left(\rho(x)\int_0^x \Delta T(x',t)\,dx'\right) \quad (15)$$

In the absence of space charge, we get

$$\Delta V(t) = \frac{\alpha_p}{\epsilon\epsilon_0}\int_0^d P(x)\,\Delta T(x,t)\,dx \quad (16)$$

In every case, the space-charge and polarization distributions can only be determined by a deconvolution process.

There is not enough physical information in the experimentally obtained data from this technique to separate space-charge and polarization components unless some basic assumptions are made. A deconvolution process imposes some limitations on the usefulness of the method (22) and care should be exercised in the interpretation of the results. It may be noted that the numerical analysis of the thermal transients obtained from the samples, thermally pulsed on both sides, can be used to an advantage for the determination of the spatial distribution profile (23).

Recently, it was shown that a simple technique of analysis of the thermal pulse data can provide good representation of the true field distribution in an electret that does not require an elaborate numerical method (24). It has been shown that the thermal pulse data, corresponding to Eq. (13), can be analyzed to provide a very good approximation of the internal field distribution profile within a corona-charged Teflon polyfluoroethylene propylene by an application of first-order differential operators (24). The field-distribution calculation can be made on line from the thermal pulse data with this method.

Thermal Wave Method: Laser Intensity Modulation

In the frequency domain, the thermal wave technique, known as the laser intensity modulation method (LIMM) may be employed to determine the spatial distributions of polarization or dipoles in dielectric materials near the surfaces (25–33). A brief outline of the method is as follows (27,28). Both surfaces of a dielectric containing unknown space-charge or polarization distributions are coated with vacuum-evaporated opaque metallic electrodes. The sample is mounted in an evacuated sample chamber containing optical windows through which radiant energy can be admitted. Each surface of the sample is exposed, in turn, to a He–Ne laser beam ($\lambda = 0.633$ nm, 5 mW) that is intensity modulated in a sinusoidal manner by means of an electromechanical chopper or an acousto-optic modulator. This causes a sinusoidal fluctuation in temperature of the metallic electrode on the sample surface, resulting in a propagation of temperature waves into the bulk of the dielectric. The temperature waves are attenuated and retarded in phase as they progress through the sample, thus providing a nonuniformly distributed thermal force that interacts with the spatially distributed polarization or space charge to produce a sinusoidal pyroelectric current. The real and imaginary parts of this current are measured with a lock-in amplifier whose reference phase is provided by the same frequency generator that drives the electromechanical or acousto-optic modulator. Figure 3 provides a schematic representation of the experimental arrangement of LIMM (28). The frequency of modulation can be varied from 20 Hz to 100 kHz and the temperature fluctuation penetrates successively to shallower depths as the laser modulation frequency is increased (28). It should be noted that the total amount of energy deposited by the laser beam is independent of frequency. The method is modeled (28,30–34) by two Fredholm equations of the first kind:

$$\frac{I_L}{I_0} = 1 + C_1 \int_0^1 P^*(y) \left(\frac{V \cosh vy}{\sinh v} \right) dy + C_2 \int_0^1 \rho(y) \left(\frac{\sinh vy}{\sinh v} - y \right) dy \tag{17}$$

and

$$\frac{I_z}{I_0} = 1 + C_1 \int_0^1 P^*(y) \left(\frac{v \cosh[v(1-y)]}{\sinh v} \right) dy - C_2 \int_0^1 \rho(y) \left(\frac{\sinh[v(1-y)]}{\sinh v} - (1-y) \right) dy \tag{18}$$

where

$$v = \left(\frac{\omega}{2k} \right)^{1/2} L(1+i) \tag{19}$$

$$C_1 = \frac{\alpha_p + \alpha_x - \alpha_E}{p} \tag{20}$$

$$C_2 = \frac{\alpha_x - \alpha_\epsilon}{p} L \tag{21}$$

Here I_0 is the current I at zero frequency, L the sample thickness, and k the thermal diffusivity. I_L is the pyroelectric current when the modulated laser beam impinges on the surface at $x = L$, I_z the current when the beam is incident on $x = 0$, p the pyroelectric coefficient, ω the angular frequency, and the

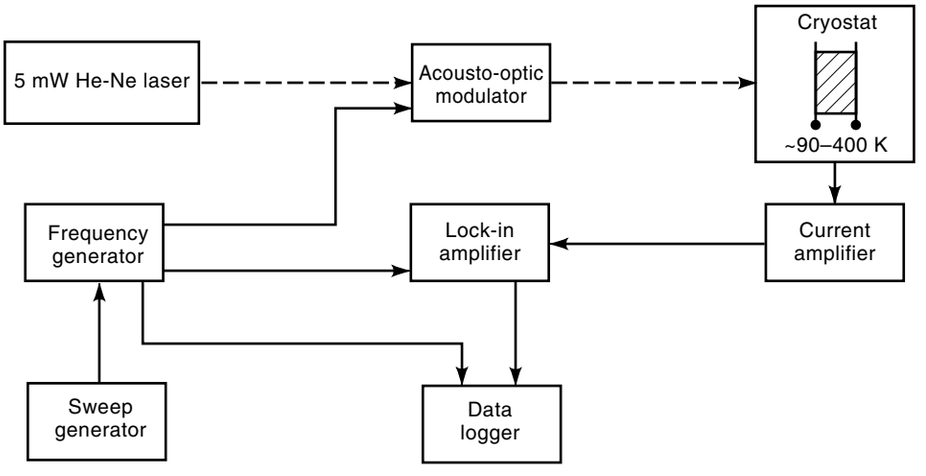

Figure 3. Schematic diagram of experimental apparatus (Ref. 28).

other symbols have been defined before. Using a coordinate x to represent the distance inside the thickness from $x = 0$ to $x = L$ and with $y = x/L$, the unknown distribution of polarization $P^*(y)$, measured as a deviation from the mean P_0, or the space charge are to be found. Once again, there is not enough physical information in the LIMM experiment, as in the case of thermal pulse method, to separate out $\rho(y)$ and $P^*(y)$ from Eqs. (17) and (18). Furthermore, Fredholm equations of the first kind are well known (35) for their characteristic numerical instability. There is a wide range of functions $\rho(y)$ and $P^*(y)$ which will satisfy Eqs. (17) and (18) within the limits of experimental errors. To resolve these difficulties, it is necessary to assume further information to some preconceived physical factors (30,32,34). However, it has been shown that in numerical evaluation with a wide range of integration together with a least-square minimization (i.e., minimization of the sum of the squared differences between the measured and the computed values), the errors in the determination of spatial charge or potential distribution can be reduced significantly (30,32–34). The LIMM has been used successfully to determine spatial distributions of polarization and space charges in ceramics (35) and polymers (33,34,36). Furthermore, the differential operator (24), mentioned earlier, can also be used to improve the resolution of deconvolution of the LIMM data near the surface region (36). The LIMM has also been used to determine the spatial distribution of polarization in a multilayer polymer system (37). It has been shown (38) that if the LIMM measurements are extended to a frequency of 0.1 MHz, a near-surface resolution of 0.3 μm can be obtained by an appropriate deconvolution procedure. The LIMM measurements up to 1.6 kHz offer only a corresponding near-surface resolution of 3 μm to 5 μm (38).

Thermal Step Method

In this method a thermal step is applied across an insulator to obtain a current response due to a thermal expansion of the sample. This current, which appears in the external circuit connecting the two electrodes of the insulators, is related to the space charge stored in the sample and is used to determine the spatial distribution of electric field and space charge (39–41). Like the thermal pulse and the thermal wave techniques, this method is also nondestructive; however, it can be applied to thick insulators (i.e., power distribution cables) in the thickness range of 2 m $\times$ 10^{-3} m to 2 $\times$ 10^{-2} m (42). The thermal step is produced by keeping one electrode of the insulator at -10°C while raising the temperature of the other electrode to 20°C.

The validity of the method has been successfully demonstrated by determining the spatial distribution of real charges deposited in a well-localized zone of an insulator by corona discharges, the electrical and thermal parameters (ϵ, x_0, L, W, α, and D) being known (41).

Recently an alternative method known as the inverse matrix technique has been successfully employed (43) to deconvolute the data obtained by the thermal step method. It is claimed that this technique requires less computational time (43) than the Fourier analysis (41) and provides significantly higher resolution and more details of space charge than those obtained by Fourier deconvolution (41).

Pressure-Pulse Method

There are several established techniques that utilize pressure pulses to determine the spatial distributions of polarization and charge in the thickness direction of dielectric materials. In these methods a propagation of ultrasonic pulse through the bulk of dielectric is employed as the physical process of investigation, and a pressure discontinuity acts as a virtual probe to detect the time-dependent changes in measurable parameters, such as charges and potentials on the electrodes (44). Each of these methods, however, will be reviewed separately in this section. The general principle of the pressure wave propagation method is as follows (45).

A pressure wave is applied uniformly on one face of a sample through a target electrode, as shown in Fig. 4 (45,46). As the wave front of the pressure wave propagates through the sample containing space charges, the relative permittivity ϵ_r of the compressed region is modified, and in addition the charges are also displaced. These two effects generate a change of the induced charges on the sample electrodes, which in turn provides either an open-circuit voltage $V(t)$ or a short-circuit current $I(t)$. The space-charge distribution $\rho(z)$, or the field distribution $E(z)$, in the bulk of the sample, and the pressure profile $P(z, t)$ are directly related to the time evolution of $V(t)$ and $I(t)$, which are given by (45,47)

$$V(t) = XG(\epsilon_r) \int_0^z E(z, 0)P(z, t)\, dz \tag{22}$$

and

$$I(t) = XC_0G(\epsilon_r) \int_0^{zt} E(z, 0) \frac{\partial P(z, t)}{\partial t}\, dz \tag{23}$$

where X is the compressibility of the dielectric material, $G(\epsilon_r)$ a function of the relative permittivity, z_f the abscissa of the wave front ($=vt$), v the velocity of sound, C_0 the capacitance of the noncompressed sample ($= \epsilon_0\epsilon_r A/d$), ϵ_0 the permittivity of free space, A the electrode area, and d the sample

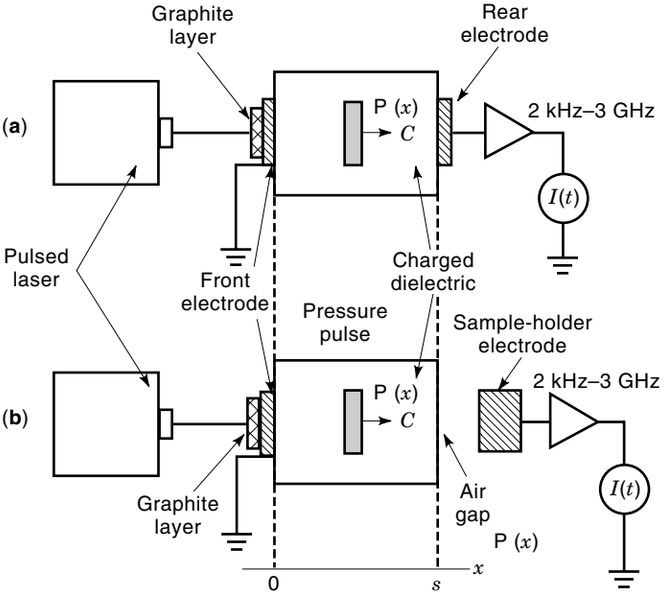

Figure 4. Schematic setup of the LIPP experiments (a) for samples metallized on both sides; (b) for samples metallized on one side (Ref. 49).

thickness. Thus the spatial distribution of the electric field $E(z)$ can be determined from a measurement of $V(t)$ or $I(t)$ if the pressure profile $P(z, t)$ is known. Furthermore, the space-charge profile $P(z)$ can be determined as it is related to $E(z)$ by Poisson's equation.

Laser-Induced Pressure-Pulse Method. In this method (48–63) the surface of a sample containing space charges is irradiated by a short laser pulse, causing an ablation of a graphite layer which is deposited on the surface prior to the experiment. This mechanical excitation following the emission of the material provides a recoil that launches a desired pressure pulse of duration τ that propagates through the sample with the velocity of sound c (see Fig. 4). A Q-switched neodymium-doped yttrium aluminium garnet (Nd:YAG) laser of wavelength 1.064 μm of peak power 1 GW, corresponding to an energy of up to 100 mJ of a single pulse with duration of 70 ps, is used. The cross-sectional area of the laser beam is approximately 0.2 cm^2. Assuming that the $c\tau$, that is, the length of the laser-induced pressure pulse (LIPP), is less than the linear dimension of the changes in the space-charge distribution of the sample, the open-circuit voltage $V(t)$ created by the pressure pulse is given by (49)

$$V(t) = -(2 - \epsilon^{-1})\chi Pc\tau E(ct) \tag{24}$$

where $E(ct) = E(x)$ is the local electric field in the sample and ϵ the permittivity. Differentiating Eq. (24) with respect to time and using Poisson's equation [$\epsilon\epsilon_0 dE/dx = \rho(x)$] with $dx = cdt$ gives the following expression:

$$\frac{dV(t)}{dt} = -\frac{1}{\epsilon\epsilon_0}\left(2 - \frac{1}{\epsilon}\right)\chi Pc^2\tau\rho(x) \tag{25}$$

Equation (25) shows the relationship between the time derivative of the open-circuit voltage to the charge density.

For short-circuit conditions with two-side-metallized samples, dV/dt is replaced by $I(t)/C$, where C is the sample capacitance and $I(t)$ is given by (49)

$$I(t) = -(2 - \epsilon^{-1})\chi Pc^2\tau(A/s)\rho(x) \tag{26}$$

where A is the sample area and s its thickness. Thus if the pressure amplitude P is known $\rho(x)$ can be directly determined from a measurement of the short-circuited current $I(t)$. The LIPP method has been successfully used (54–58) for the determination of spatial distribution of space charges and polarization in thin films of polyethylene terephthalate (PET), polyfluoroethylene propylene (FEP), polyamide (PI), and polyvinylidene fluoride (PVDF) (52). The LIPP method has also been used to determine the space-charge profiles in thick slabs of (>1 mm) for low-density polyethylene (59) and thick films of cross-linked polyethylene (61). The resolution of this method is at best approximately 1 μm.

It is of interest to note that the spatial distribution of charges injected by monoenergetic electrons in Teflon FEP has been determined by both LIPP and LIMM (33). A comparison of the results provided by these two different techniques shows good agreement (33).

Thermoelastically Generated LIPP. A variation of LIPP is a technique that can generate thermoelastic stress waves in a transparent solid dielectric containing an optically absorbing layer when it is suddenly illuminated by a subnanosecond (300 ps) laser pulse (64–67). As a result there is an abrupt increase in the spatially dependent temperature, which is proportional to the distribution of absorbed energy. At the moment of energy absorption the dielectric is constrained inertially against thermal expansion, and a compressive stress wave, which is proportional to the local temperature increment, appears. This stress is subsequently relaxed by a propagation of planar, longitudinal acoustic pulses that replicate the initial pulses. Each of these pressure pulses takes away half of the mechanical displacement required to relax the heater region (64). A numerical deconvolution process is required to determine the spatial distribution. It has been claimed that the sensitivity and the resolution of the method is approximately 10 μC/m^2 and $\sim$1 μm, respectively (64). A numerical deconvolution is required to determine the spatial distribution of space charges and polarization from the measured data. This technique has been employed to determine space-charge mapping and the internal fields in metal-PET-metal samples (65) and in PET and polystyrene capacitor structures (66).

Pressure-Wave Propagation Method. In the pressure-wave propagation (PWP) method (45,47,67–72), the pressure wave is generated by an impact of a 35 ps Nd:YAG laser on a 500 μm thick aluminum target bonded to a dielectric plate under investigation. The spatial distribution of field and charge density may be obtained.

The PWP technique has been used to determine the space-charge and polarization distributions of 50 μm to 200 μm thick polymer electrets (45,69,71) and high-voltage polyethylene cables (70,72,73). It has also been used to determine surface charge distribution (74).

Laser-Generated Acoustic Pulse Method. An acoustic pulse may be generated by a HV spark between a conductor and a diaphragm to compress locally a dielectric material (75). However, this method has poor sensitivity and resolution, as such a pulse source is not very reproducible and has insufficient bandwidth and a high ratio of low-frequency energy to high-frequency energy. These difficulties can be overcome by using a laser as a source of power to generate acoustic pulses (75,76) when the incident laser beam is absorbed in a thin paper target coupled to the sample under investigation.

Acoustic Probe Method. In this method (77–83) longitudinal pressure waves of 100 ns duration are generated by ablation, and thermal stress effects follow irradiation of a graphite disk with a Q-switched ruby laser whose 30 ns pulses provide an energy density of 0.5 J/cm^2. The longitudinal waves thus produced deform a narrow layer of the sample, and electrical signals are produced by the mechanical excitation of the charged specimen. It has been claimed that the resolution of the method is $\sim$0.2 mm (83,84). This technique has been used to determine space-charge and field distributions in insulators charged by electron, proton, and α-particle radiation (77,79,80,83,85).

Piezoelectrically Generated Pressure Step. The piezoelectrically generated pressure-step (PPS) technique (86–90) is based on the propagation of an acoustic step wave through a

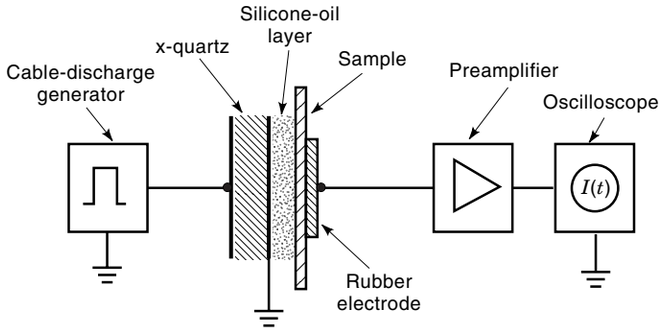

Figure 5. Experimental setup for the piezoelectrically generated pressure-step (PPS) method. The same arrangement is used for the piezoelectrically generated pressure-pulse (PPP) technique (Ref. 90).

sample under investigation. Figure 5 shows schematically the experimental arrangement (90) of the method in which a 100 ns long square pulse of amplitude 400 V to 600 V is generated by a relay-triggered discharge of a coaxial cable. This step voltage drives a piezoelectric quartz plate of 25 mm in diameter and 3 mm in thickness. A silicone oil layer of thickness 100 nm to 200 nm is employed to couple the resulting pressure step to the sample, the other surface of the unmetallized sample being contacted by a conducting rubber disk of ~5 mm in diameter. The electrical response of the sample is detected between the rubber electrode and the metallized quartz, the latter being grounded. It may be shown that the short-circuit current $I(t)$ at time t and electric field $E(x)$ at a location $x = ct$ of the pressure step of the sample is given by (88)

$$I(t) = \frac{\epsilon_0 \epsilon_r A}{s}\left(\frac{4}{3} + \frac{\epsilon_r}{3} - \frac{2}{3\epsilon}\right)\frac{P}{\rho_0 c}E(ct) \tag{27}$$

where ϵ_r, ρ, S, and A are the relative permittivity, the density, the thickness, and the electrode area of the sample, respectively, ϵ_0 the vacuum dielectric constant, c the velocity of the longitudinal sound waves, and P the amplitude of the pressure step. An alternative expression for $I(t)$ using the electrostriction coefficient γ is (86)

$$I(t) = \frac{A}{s}(1+\gamma)v\int_0^{x=ct}\rho(z)\,dz \tag{28}$$

where

$$\gamma = -\frac{1}{\epsilon}\frac{\partial \epsilon}{\partial s} \tag{29}$$

s is the mechanical strain, $\rho(z)$ the charge distribution, and γ the particle velocity in the step wave ($v = P/\rho_0 c$).

Combining all the unchanged parameters into a single constant C, Eqs. (28) and (29) may thus be rewritten (90)

$$I(t) = CE(ct) = \frac{C}{\epsilon_0 \epsilon}\int_0^{x=ct}\rho(z)\,dz \tag{30}$$

The present resolution of this technique is ~1 μm for the determination of the location of charge layers. The spatial field and polarization distributions can be directly scanned with the PPS method.

Pulsed Electro-Acoustic Method

The principle of the pulsed electro-acoustic method (PEA) is based on the Lorentz force law whereby an externally applied pulse field induces a perturbing force density on a dielectric containing resident charges (91–111). This perturbation produces an acoustic wave that originates from the charges in the bulk. The acoustic signal is then detected by a broadband piezoelectric sensor, located on one of the electrodes (96). The charge distribution in the dielectric may be obtained in real time from the output voltage of the piezoelectric sensor following a digital signal processing effort. This method has been successfully applied to determine spatial distribution of charges in cross-linked polyethylene (XLPE) coaxial cables (109).

Other Methods

A detection of photocurrents can provide information on the space-charge distribution (112–114). Electro-optical methods, namely, Kerr (112–125) and Pockel effects (126), have been used to detect space charges in dielectric liquids (116–120) and polymers (121–125). Furthermore, spectroscopic methods, such as Stark (127) and Raman spectroscopy (128) have also been attempted to measure space charges in dielectric materials. However, these methods have yet to receive an acceptable measure of understanding and reliability in the determination of spatial space-charge density.

Monoenergetic electron-beam probing techniques (129–133) have been employed to scan sample thicknesses to evaluate space-charge concentrations in the irradiated regions of insulators. However, these methods, which require a definitive knowledge of charge carrier mobility that may vary spatially, are also destructive, which limits their applications.

It is established that suitable solvents may diffuse into a dielectric, thus creating a higher charge carrier mobility in the diffusion region (134,135). As a result there will be a charge migration in this region, and this can be detected electrically in an external circuit. However, as many assumptions need to be made, the diffusing chemical solvent method may be limited in some cases only for the determination of the space-charge distribution.

Several attempts (136–138) have been made to utilize the well-established capacity field probe techniques (139–142) to detect space charges. Materials have been mechanically sliced and charges on each slice have been measured (136,137). Apart from being a destructive method for such an approach, it is difficult to determine true charge distribution as the effect of the cutting tool on the charge distribution is not known.

A multipoint measurement technique (138) that measures charges on the whole surface for different probes to surface clearances can be employed. The distribution of the charge density may be determined from the probe responses using an appropriate numerical field calculation.

CONCLUSION

The techniques such as the thermal pulse, thermal wave (LIMM), thermal step, and the pressure-pulse methods including laser-induced pressure pulse (LIPP), pressure-wave propagation (PWP), piezoelectrically generated pressure-step

(PPS), and the pulsed electro-acoustic (PEA) methods are the major developments in recent years for the determination of the spatial distribution of space charges and polarization in nonpolar and polar dielectric materials and particularly in insulating polymeric solids. Table 1 provides an overview of the methods and their capabilities (46).

The thermal pulse method relies on the diffusion of heat and the thermal wave (LIMM) uses the concept of a frequency-dependent steady-state heat profile. Both these methods are quick and easy to use, but a numerical deconvolution is required in each case. The LIMM has particularly high resolution near the film surface. For both these cases the film thickness is limited ($\leq$200 μm). It appears in most cases, except for the LIPP method, that either a numerical deconvolution of the experimental data is required (i.e., thermostatically generated LIPP, laser-generated acoustic pulse method, piezoelectrically generated pressure-step method, thermal step method, and electro-acoustic stress pulse method) or the resolution can be improved with deconvolution (pressure wave propagation method) for the determination of spatial distribution of charges and polarization. The pressure-wave propagation method can also be used for surface charge measurements. The LIPP, PEA, and PPS and thermal step methods are suitable for space-charge profile determination in thick samples and appear to be quite promising in scanning space charges in thick polymeric power distribution cables.

Table 1. Overview of Methods and Capabilities: l is the method's resolution, and s is the sample thickness[a]

Method	Disturbance	Scan Mechanism	l (μm)	s (μm)	Comments
Thermal pulse method	Absorption of short light pulse in front electrode	Diffusion according to heat-conduction equation	$\geq$2	$\sim$200 2,000–20,000	High resolution requires deconvolution
Laser intensity modulation method	Absorption of modulated light in front electrode	Frequency-dependent steady-state heat profile	$\geq$2	$\sim$25	Numerical deconvolution is required
Laser induced pressure pulse method	Absorption of short laser light pulse in front electrode	Propagation with longitudinal sound velocity	1	100–1,000	No deconvolution is required
Thermoelastically generated LIPP	Absorption of short laser light pulse in thin buried layer	Propagation with longitudinal sound velocity	1	50–70	Deconvolution is required
Pressure wave propagation method	Absorption of short laser light pulse in metal target	Propagation with longitudinal sound velocity	10	5–200	Resolution improved with deconvolution. Also used for surface charge measurements
Nonstructured acoustic pulse method	HV spark between conductor and metal diaphragm	Propagation with longitudinal sound velocity	1,000	$\leq$10,000	Used for solid and liquid dielectric. Higher resolution with deconvolution
Laser-generated acoustic pulse method	Absorption of short laser light pulse in thin paper target	Propagation with longitudinal sound velocity	50	$\leq$3,000	Deconvolution is required. Target and sample immersed in dielectric liquid
Acoustic probe method	Absorption of laser light pulse in front electrode	Propagation with longitudinal sound velocity	200	2,000–6,000	
Piezoelectrically generated pressure step method	Electrical excitation of piezoelectric quartz plate	Propagation with longitudinal sound velocity	1	25	Deconvolution is required
Thermal step method	Applying two isothermal sources across sample	Thermal expansion of the sample	150	2,000–20,000	Deconvolution is required
Electro-acoustic stress pulse method	Force of modulated electric field on charges in sample	Propagation with longitudinal sound velocity	100	$\leq$10,000	Deconvolution is required. Also used for surface charge measurements
Photoconductivity method	Absorption of narrow light beam in sample	External movement of light beam	$\geq$1.5	—	Nondestructive for short illumination time
Space-charge mapping	Interaction of polarized light with field	Parallel illumination of sample or movement of light beam	200	—	Mostly used on transparent dielectric liquids
Spectroscopy	Absorption of exciting radiation in sample	External movement of radiation source or sample	$\geq$50	—	Few applications
Field probe	None	Capacitive coupling to the field	1,000	$\leq$20,000	Destructive

[a] *Source:* References 28, 46.

BIBLIOGRAPHY

1. H. R. Zeller and R. W. Schneider, Electrofracture mechanics of dielectric ageing, *J. Appl. Phys.,* **56**: 455–459, 1985.
2. M. Mammeri, C. Laurent, and J. Salon, Influence of space charge buildup on the transition to electrical treeing in PE under ac voltage, *IEEE Trans. Dielectr. Electr. Insul.,* **2**: 27–35, 1995.
3. L. Dissado, G. Mazzanti, and G. C. Montanari, The incorporation of space charge degradation in the life model for electrical insulating materials, *IEEE Trans. Dielectr. Electr. Insul.,* **2**: 1147–1158, 1995.
4. G. V. Barbosa-Canovas and B. G. Swanson, Space charge evolution in dilute binary electrolytes exposed to HIV transients, *IEEE Trans. Dielectr. Electr. Insul.,* **3**: 747–753, 1996.
5. E. B. Baker and H. A. Boltz, Thermionic emission into dielectric liquids, *Phys. Rev.,* **51**: 275–282, 1937.
6. R. Kressmann, G. M. Sessler, and P. Gunter, Space charge electrets, *IEEE Trans. Dielectr. Electr. Appl.,* **3**: 607–623, 1996.
7. G. M. Sessler (ed.), *Electrets,* in *Topics in Applied Physics,* 2nd ed., vol. 33, Berlin: Springer Verlag, 1987.
8. R. Gerhard-Multhaupt, Dielectrics with quasi-permanent charges or polarization, *IEEE Trans. Electr. Insul.,* **22**: 531–554, 1987.
9. J. F. Gibbons, *Semiconductor Electronics,* New York: McGraw-Hill, 1996, p. 223.
10. J. D. Cobine, *Gaseous Conductors,* New York: Dover Publications Inc., 1958, p. 128.
11. D. R. Lamb, *Electrical Conduction Mechanisms in Thin Insulating Films,* London: Methuen, 1987, chap. 4, pp. 22–27.
12. M. A. Lampert, Simplified theory of space-charge-limited currents in an insulator with traps, *Phys. Rev.,* **103**: 1648–1656, 1956.
13. M. A. Lampert, Volume controlled current injection in solids, *Rep. Prog. Phys.,* **27**: 329–367, 1964.
14. J. van Turnhout, Thermally stimulated discharge of electrets, in G. M. Sessler (ed.), *Applied Physics: Electrets,* 2nd enlarged ed., New York: Springer Verlag, 1987, chap. 3, pp. 81–215.
15. S. J. Carr, Thermally stimulated discharge current analysis, in D. A. Seaner (ed.), *Electrical Properties of Polymers,* London: Academic Press, 1982, chap. 5, pp. 215–240.
16. J. Vanderschuren and A. Linken, Thermally stimulated depolarization and dielectric losses in polymers. Some problems posed by the comparison of activation energies, *J. Electrostatics,* **3**: 155–161, 1977.
17. R. E. Collins, Distribution of charge in electrets, *Appl. Phys. Lett.,* **26**: 675–677, 1975.
18. R. E. Collins, Analysis of spatial distribution of charges and dipoles in electrets, *J. Appl. Phys.,* **47**: 4804–4808, 1976.
19. R. E. Collins, Measurement of charge distribution in electrets, *Rev. Sci. Instrum.,* **48**: 83–91, 1977.
20. A. S. De Reggi et al., Determination of charge or polarization distribution across polymer electrets by thermal pulse method and Fourier analysis, *Phys. Rev. Lett.,* **40**: 413–416, 1978.
21. H. von Seggern, Thermal pulse technique for determining charge distribution: Effect of measurement accuracy, *Appl. Phys. Lett.,* **33**: 134–137, 1978.
22. R. E. Collins, Practical application of the thermal pulsing technique to the study of electrets, *J. Appl. Phys.,* **51** (6): 2973–2986, 1980.
23. F. I. Mopsik and A. S. De Reggi, Numerical evolution of the dielectric polarization distribution from thermal pulse data, *J. Appl. Phys.,* **53** (6): 4333–4339, 1982.
24. S. Bauer, Method for the analysis of thermal-pulse data, *Phys. Rev. B,* **47** (17): 11049–11055, 1993.
25. S. B. Lang and D. K. Das-Gupta, A technique for determining the polarization distribution in thin polymer electrets using periodic heating, *Ferroelectrics,* **39**: 1249–1252, 1981.
26. S. B. Lang and D. K. Das-Gupta, Complex polarization distributions in PVDF samples, *Ferroelectrics,* **55**: 151–154, 1984.
27. S. B. Lang and D. K. Das-Gupta, A new technique for determination of the spatial distribution of polarization in polymer electrets, *Ferroelectrics,* **60**: 23–36, 1984.
28. S. B. Lang and D. K. Das-Gupta, Laser intensity modulation method: A technique for determination of spatial distributions of polarization and space charge in polymer electrets, *J. Appl. Phys.,* **59** (6): 2151–2160, 1986.
29. S. B. Lang, New theoretical analysis for the laser intensity modulation method (LIMM), *Ferroelectrics,* **106**: 269–274, 1990.
30. D. K. Das-Gupta and J. S. Hornsby, A non-destructive technique for the determination of spatial charge and polarization distributions in insulating polymers, *J. Phys. D: Appl. Phys.,* **23**: 1485–1490, 1990.
31. S. B. Lang, Laser intensity modulation method (LIMM): Experimental techniques theory and solution of the integral equation, *Ferroelectrics,* **118**: 343–361, 1991.
32. D. K. Das-Gupta and J. S. Hornsby, Laser intensity modulation method (LIMM): An analytical and numerical modification, *IEEE Trans. Electr. Insul.,* **26** (1): 63–68, 1991.
33. D. K. Das-Gupta et al., Comparison of charge distributions in FEP measured with thermal wave and pressure pulse technique, *J. Phys. D: Appl. Phys.,* **29**: 3113–3116, 1996.
34. M. Wübbenhorst et al., Spatial distribution of polymerization in polyethylene, Ac aged in humid environment, *Proc. ISE9,* Shanghai, China, September, 1996.
35. S. B. Lang and Q. R. Yin, Spatial distributions of polarization and space charges in tin-substituted in lead zarconate titanate using laser intensity modulation method, *Ferroelectrics,* **74**: 357–368, 1987.
36. B. Ploss, R. Emmerich, and S. Bauer, Thermal wave probing of pyroelectric distributions in the surface region of ferroelectric materials: A new method of analysis, *J. Appl. Phys.,* **72** (11): 5363–5370, 1992.
37. P. Bloss and H. Schäffer, Investigations of polarization profiles in multilayer systems by using the laser intensity modulation method, *Rev. Sci. Instrum.,* **65** (5): 1541–1549,1994.
38. P. Bloss et al., A comparison of space-charge distributions in electron-beam irradiated FEP obtained by using heat-wave and pressure pulse techniques, *J. Phys. D: Appl. Phys.,* **30**: 1665–1675, 1997.
39. A. Toureille and J. P. Reboul, The thermal step technique applied to the study of charge decay in polyethylene thermoelectrets, *Proc. 6th Int. Symp. Electrets (ISE 6),* Oxford, 1988.
40. A. Toureille, J. P. Reboul, and P. Merle, Determination des densites de charge d'espace dans les isolants solids par la methode de l'onde thermique, *J. Phys. (Paris),* **III**: 111–123, 1991.
41. A. Cherifi, M. Abou Dakka, and A. Toureille, The validation of the thermal step method, *IEEE Trans. Electr. Insul.,* **27**: 1152–1158, 1992.
42. A. Toureille et al., Determination des densites de charge charge d'espace dans un cable haute tension a forte, apaisseur d'isolant par la methode de l'onde thermique, *Rev. Phys. Appl.,* **25**: 405–408, 1990.
43. M. Abou-Dakka, S. S. Bamji, and A. T. Bulinski, Space-charge distribution in XLPE by TSM, using the inverse matrix technique, *IEEE Trans. Dielectr. Electr. Insul.,* **4**: 314–320, 1997.

44. P. Laurenceau, G. Dreyfus, and J. Lewiner, New principle for the determination of potential distributions in dielectrics, *Phys. Rev. Lett.,* **38**: 46–49, 1977.
45. M. P. Cals, J. P. Marque, and C. Alquie, The pressure-pulse method for measuring space-charge distribution in irradiated insulators, *IEEE Trans. Electr. Insul.,* **24**: 999–1003, 1989.
46. N. H. Ahmed and N. N. Srinivas, Review of space charge measurements in dielectrics, *IEEE Trans. Dielectr. Electr. Insul.,* **4**: 644–656, 1997.
47. C. Alquié, J. Lewiner, and G. Dreyfus, Stress-wave probing of electric field distributions in dielectrics, *Phys. Rev. Lett.,* **47**: 1483–1487, 1981.
48. G. M. Sessler and R. Gerhard-Multhaupt, A review of methods for charge or field distribution studies on radiation charged dielectric films, *Radiat. Phys. Chem.,* **23**: 363–370, 1984.
49. G. M. Sessler, J. E. West, and G. Gerhard, High resolution laser pulse method for measuring charge distributions in dielectrics, *Phys. Rev. Lett.,* **48** (8): 563–566, 1982.
50. G. M. Sessler et al., Nondestructive laser method for measuring charge profiles in irradiated polymer films, *IEEE Trans. Nucl. Sci.,* **NS-29**: 1644–1649, 1982.
51. R. Gerhard-Multhaupt, Analysis of pressure wave methods for the non-destructive determination of spatial charge or field distributions in dielectrics, *Phys. Rev. B,* **27** (4): 2494–2503, 1983.
52. R. Gerhard-Multhaupt, G. M. Sessler, and J. E. West, Investigation of piezoelectricity distribution in poly(vinylidene fluoride) by means of quartz- or laser generated pressure pulses, *J. Appl. Phys.,* **55** (7): 2769–2775, 1984.
53. G. M. Sessler et al., Optoacoustic generation and electrical detection of subnanosecond acoustic pulses, *J. Appl. Phys.,* **58** (1): 119–121, 1985.
54. G. M. Sessler et al., Charge and polarization profiles in polymer electrets, *IEEE Trans. Electr. Insul.,* **21**: 411–415, 1986.
55. G. M. Sessler et al., Charge and polarization profiles in polymer electrets, in *Proc. 5th Int. Symp. Electrets,* Heidelberg, 1985, pp. 565–570.
56. J. E. West et al., Space charge distribution in electron beam charge Mylar and Kapton films, *IEEE Trans. Electr. Insul.,* **24**: 533–536, 1989.
57. G. M. Sessler, Charge storage in dielectrics, *IEEE Trans. Electr. Insul.,* **24**: 395–402, 1989.
58. L. Tingi and G. M. Sessler, An experimental study of charge distribution in electron beam irradiated polypropylene films, *IEEE Trans. Electr. Insul.,* **26**: 228–235, 1991.
59. Y. Suzuoki et al., Study of space charge in polyethylene by direct probing, *IEEE Trans. Electr. Insul.,* **26**: 1073–1079, 1991.
60. T. Mizutani et al., Direct observation of space charge distribution in polyethylene, *1989 Annu. Rep. Conf. Electr. Insul. Dielect. Phenom.,* 1989, pp. 309–314.
61. Y. Suzuoki et al., Study of space charge in polyethylene in laser induced pressure pulse technique, *1990 Annu. Rep. Conf. Electr. Insul. Dielectr. Phenom,* 1990, pp. 203–207.
62. Y. Suzuoki et al., Study of effects of space charge in polyethylene by its direct probing, *Conf. Rec. 1990 IEEE Int. Symp. Electr. Insul.,* 1990, pp. 401–404.
63. M. Ieda, M. Nagao, and M. Hikita, Recent progress of high field conduction and breakdown in insulating polymers, in *Proc. 4th Int. Conf. Conduction Breakdown Solid Dielectrics,* 1992, pp. 383–392.
64. R. A. Anderson and S. R. Kurtz, Direct observation of field-injected space charge in a metal-insulator-metal-structure, *J. Appl. Phys.,* **56**: 2856–2863, 1984.
65. R. A. Anderson and S. R. Kurtz, Properties of the metal-polymer interface observed with space charge mapping techniques, *J. Appl. Phys.,* **60**: 681–687, 1986.
66. R. A. Anderson and S. R. Kurtz, Radiation induced space charge in polymer film capacitors, *Appl. Phys. Lett.,* **49**: 1484–1486, 1986.
67. C. Alquié, J. Lewiner, and G. Dreyfus, Analysis of laser induced acoustic pulse probing of charge distributions in dielectrics, *J. Phys. Lett.,* **44**: 171–178, 1983.
68. C. Alquié and J. Lewiner, A new method for studying piezoelectric materials, *Rev. Phys. Appl.,* **20**: 395–402, 19xx.
69. C. Alquié, F. Chapeau, and J. Lewiner, Evolution of charge distributions in FEP films analyzed by the laser induced acoustic pulse method, *1984 Annu. Rep. Con. on Electr. Insul. Dielectr. Phenom.,* IEE Report No. 84CH1994-3, 1984, pp. 488–496.
70. F. Chapeau, C. Alquié, and J. Lewiner, The pressure wave propagation method for the analysis of insulating materials: Application to LDPE used in HV cables, *IEEE Trans. Electr. Insul.,* **21**: 405–410, 1986.
71. C. Laburthe-Tolra, C. Alquié, and J. Lewiner, Piezoelectricity analysis in VDF-TrFE copolymer films using the pressure wave propagation method, *1990 Annu. Rep. Conf. Electr. Insul. Dielectr. Phenom.,* 1990, pp. 71–77.
72. T. Ditchi et al., Electrical properties of electrode/polyethylene/electrode structures, *IEEE Trans. Electr. Insul.,* **24**: 403–408, 1989.
73. F. Chapeau et al., Comparative study of the behavior of two polyethylene types under dc voltage, by the pressure wave method, *Conf. JICABLE 1987,* Versailles, France, 1987, pp. 81–97.
74. F. Chapeau et al., Pulsed laser determination of surface electric charge distributions, *J. Phys. Lett.,* **43**: 687–693, 1982.
75. A. Migliori and J. D. Thompson, A nondestructive acoustic electric field probe, *J. Appl. Phys.,* **51**: 479–485, 1980.
76. A. Migliori and T. Holfler, Use of laser generated acoustic pulses to measure the electric field inside a solid dielectrics, *Rev. Sci. Instrum.,* **33**: 662–666, 1982.
77. A. G. Rozno and V. V. Gromov, Formation and relaxation of space charge during electron irradiation of some dielectrics, *Russ. J. Phys. Chem.,* **54**: 1482, 1980.
78. A. G. Rozno and V. V. Gromov, Electric field distribution in high resistance solid radiative materials, *Russ. J. Phys. Chem.,* **55**: 901–902, 1981.
79. A. G. Rozno and V. V. Gromov, Electric charge in irradiated polyethylene, *Radiat. Phys. Chem.,* **22**: 555–564, 1983.
80. A. G. Rozno and V. V. Gromov, Direct measurement of the volume electrification in irradiated dielectrics, *Radiat. Phys. Chem.,* **23**: 295–304, 1984.
81. A. G. Rozno and V. V. Gromov, Electric charge in the volume of radioactive dielectrics, *Radiat. Phys. Chem.,* **23**: 307–317, 1984.
82. O. V. Andreyev, V. I. Vereltenic, and O. B. Evdokimov, Probing methods of strong current fields in high resistance dielectrics, *Radiat. Phys. Chem.,* **23**: 349–358, 1984.
83. U. Decker, L. Richter, and J. Box, Aspects of radiation induced charge accumulation in dielectrics, *Radiat. Phys. Chem.,* **26**: 579–581, 1985.
84. A. G. Rozno and V. V. Gromov, Measurement of the space charge distribution in solid dielectrics, *Sov. Tech. Phys. Lett.,* **5**: 266–267, 1979.
85. A. G. Rozno and V. V. Gromov, Electric charge distribution and radiation effects in irradiated dielectrics, *IEEE Trans. Electr. Insul.,* **21**: 417–425, 1986.

86. W. Eisenmenger and M. Haardt, Observation of charge compensated polarization zones in PVDF film by piezoelectric acoustic step wave response, *Solid State Commun.,* **41**: 917–920, 1982.
87. M. Haardt and W. Eisenmenger, High resolution technique for measuring charge and polarization distributions in dielectrics by piezoelectrically induced pressure step waves, *1982 Annu. Rep. Conf. Electr. Insul. Dielectr. Phenom.,* IEEE Report No. 82CH1773-1, 1982, pp. 46–51.
88. R. Gerhardt-Multhaupt, Analysis of pressure-wave methods for the non-destructive determination of spatial charge or field distribution in dielectrics, *Phys. Rev. B.* **27**: 494–503, 1983.
89. W. Eisenmenger, M. Haardt, and K. Holkik, Observation of charge compensated polarization zones in PVDF film by piezoelectrically generated pressure step wave response, *1982 Annu. Rep. Conf. Electr. Insul. Dielectr. Phenom.,* IEEE Report No. 82CH1773-1, 1982, pp. 52–57.
90. R. Gerhard-Multhaupt, W. Eisenmenger, and G. M. Sessler, Electric-field profiles in electron-beam-charged polymer electrets, *J. Phys. D,* **16**: 2247–2256, 1983.
91. T. Takada and T. Sakai, Measurement of electric fields at a dielectric/electrode/interface using an acoustic transducer technique, *IEEE Trans. Electr. Insul.,* **18**: 619–628, 1983.
92. T. Maeno, H. Kushibe, and T. Takada, Pulsed electro-acoustic method for the measurement of volume charges in e-beam irradiated PMMA, *1985 Annu. Rep. Conf. Electr. Insul. Dielectr. Phenom.,* IEEE Report No. 85CH2165-9, 1985, 389–397.
93. T. Takada, T. Maeno, and H. Kushibe, An electric stress pulse technique for the measurement of charges in a plastic plate irradiated by an electron beam, *Proc. 5th Int. Symp. Electrets,* Heidelberg, 1985, pp. 450–455.
94. T. Oda and K. Ueno, Surface charge density measurement of charged dielectric films by using supersonic vibration, *Proc. 5th Int. Symp. Electrets,* Heidelberg, 1985, pp. 488–493.
95. T. Oda and K. Ueno, Surface charge density measurement of charged dielectric films by using supersonic vibration, *IEEE Trans. Electr. Insul.,* **21**: 375–381, 1986.
96. T. Takada, T. Maeno, and H. Kushibe, An electric stress-pulse technique for the measurement of charges in a plastic plate irradiation by an electron beam, *IEEE Trans. Electr. Insul.,* **22**: 479–501, 1987.
97. M. Takashima, K. Soda, and T. Takada, Measurement of electric charges at the interface between two dielectric layers using an electro-acoustic transducer technique, *IEEE Trans. Electr. Insul.,* **23**: 287–295, 1988.
98. T. Maeno et al., Measurement of spatial charge distribution in thick dielectrics using the pulsed electroacoustic method, *IEEE Trans. Electr. Insul.,* **23**: 433–439, 1988.
99. H. Kushibe, T. Maeno, and T. Takada, Measurement of accumulated charge inside dielectric by pulsed electric forced techniques, *Trans. IEE Jpn.,* **A-100**: 118–124, 1986.
100. J. B. Bernstein and C. M. Cooke, Bulk space charge behavior in polymethylmethacrylate under an imposed virtual cathode condition, *IEEE Trans. Electr. Insul.,* **26**: 1080–1086, 1991.
101. C. M. Cooke and E. Gollin, Gas-solid interface emissions determinated by the ESAW charge detection method, in L. Christophorou and I. Saunders (eds.), *Gaseous Dielectrics VI,* New York: Plenum Press, 1991, pp. 285–296.
102. J. B. Bernstein and C. M. Cooke, Electric poling behavior of polymethylmethacrylate, *IEEE Trans. Electr. Insul.,* **26**: 1087–1093, 1991.
103. C. M. Cooke et al., Calibration of volume charge measurements by use of electron beam implantation, *Conf. Electr. Insul. Dielectr. Phenom.,* Piscataway, NJ: IEEE, 1989, pp. 435–441.
104. T. Maeno et al., Measurement and simulation of spatial charge distribution in electron-beam-irradiated polymers, *J. Appl. Phys.,* **65**: 1147–1151, 1989.
105. J. B. Bernstein, Analysis of the electrically stimulated acoustic wave method for observing space charge in semi-insulating films, *Phys. Rev. B,* **44** (19): 10804–10814, 1991.
106. K. Fugunango et al., Measurement of charge distribution in the insulation of cable using pulsed electroacoustic method, *IEE Trans. Jpn.,* **110-a** (9): 647–648, 1990.
107. M. Yasuda, M. Ito, and T. Takada, Measurement of charge distributions in coaxial cable using the pulsed electroacoustic method, *Jpn. J. Appl. Phys.,* **30**: 71–73, 1991.
108. N. Hozumi, T. Okamoto, and T. Imajo, Space charge distribution measurement in long size XLPE cable using the pulsed electroacoustic method, *IEEE Symp. Electr. Insul.,* Baltimore, 1992, pp. 294–297.
109. R. Liu, T. Takada, and N. Takasu, Pulsed electro-acoustic method in power cables under both dc and ac electric fields, *J. Phys. D,* **26**: 986–993, 1993.
110. Y. Li and T. Takada, Experimental observation of charge transport and injection in XLPE at polarity reversal, *J. Phys. D,* **25**: 704–716, 1992.
111. Y. Li, M. Yasuda, and T. Takada, Pulsed electroacoustic method for measurement of charge accumulation in solid dielectrics, *IEEE Trans. Dielectr. Electr. Insul.,* **1**: 188–195, 1994.
112. A. Dias Tavares, New method for the determination of space charge in dielectric, *J. Chem. Phys.,* **59**: 2154–2155, 1973.
113. S. G. Boev and G. I. Sigaev, Light-probe measurement of electric field strength in dielectrics charged by electron bombardment, *Instrum. Exp. Tech.,* **24**: 1054–1057, 1982.
114. T. F. Carruthers et al., Electric field distributions in planar transferred-electron devices measured with picosecond optical pulses, *IEEE Electron Devices Lett.,* **3**: 347–349, 1982.
115. O. V. Anderyev, V. I. Veretelnic, and I. B. Evdokimov, Probing methods of strong current fields in high resistance dielectrics, *Radiat. Phys. Chem.,* **23** (3): 349–358, 1984.
116. M. Zahn, T. Takada, and S. H. Voldman, Kerr electro-optic field mapping measurement in water using parallel cylindrical electrodes, *J. Appl. Phys.,* **54** (9): 4749–4761, 1983.
117. M. Zahn and T. Takada, HV electric field and space charge distribution in highly purified water, *J. Appl. Phys.,* **54** (9): 4762–4775, 1983.
118. S. M. Mahajan and T. S. Sudarshan, Measurement of the space charge field in transformer oil using its Kerr effect, *IEEE Trans. Dielectr. Electr. Insul.,* **1**: 63–70, 1994.
119. E. F. Kelly and R. E. Hebner, Electro-optic measurement of the electric field distribution in transformer oil, *IEEE Trans. Power Appar. Syst.,* **25**: 1–7, 1983.
120. A. Torne and U. Gafvesrt, Measurement of electric field in transformer oil using the Kerr technique with optical and electrical modulation, *Conf. Rec. ICPADM, IEEE 85CH2115-4,* 1985, pp. 61–64.
121. M. Zahn et al., Kerr electro-optic field mapping measurements in electron beam irradiated polymethylmethacrylate, *IEEE Trans. Electr. Insul.,* **22**: 181–195, 1987.
122. K. S. Kim, T. C. Cheng, and D. E. Copper, Kerr effect in solid polymethylmethacrylate and polyethylene, *J. Appl. Phys.,* **54** (1): 449–451, 1983.
123. M. Hikita et al., Kerr electro-optic field mapping measurements in electron-beam irradiated polymethylmethacrylate, *IEEE Trans. Electr. Insul.,* **23**: 861–880, 1988.
124. M. Hikita et al., Kerr electro-optic field and charge mapping measurements in electron-beam irradiated polymethylacrylate

in air and vacuum, *6th IEEE Pulsed Power Conf.,* Arlington, VA, 1987, pp. 653–656.

125. M. Hikita et al., Electric field and charge profiles of electron beam irradiated PMMA until breakdown using Kerr electro-optic measurements, *1987 Annu. Rep. Conf. Electr. Insul. Dielectr. Phenom.,* 1987, pp. 300–306.
126. T. Kawasaki, Y. Arai, and T. Takada, Measurement of electrical surface charge distribution on insulating material by electrooptic Pockels cell, *1990 Annu. Rep. Con. Electr. Insul. Dielectr. Phenom.,* 1990, pp. 373–378.
127. S. J. Sheng and D. M. Hanson, Spectroscopic measurement of the space charge distribution in insulators, *J. Appl. Phys.,* **45**: 4954–4956, 1974.
128. M. Latour and G. Donnet, Detection of internal field strength in polyethylene by means of ionic dopants, *J. Electrostat.,* **8**: 81–87, 1979.
129. G. M. Sessler et al., Determination of spatial distribution of charges in thin dielectrics, *Phys. Rev. Lett.,* **XX**: 368–371, 1977.
130. D. W. Tong, Electron beam probing of space charge in PET films, *IEEE Trans. Electr. Insul.,* **17**: 377–385, 1982.
131. G. M. Sessler, J. E. West, and H. Seggern, Electron beam method for detecting charge distribution in thin polyethyleneterephthalate films, *J. Appl. Phys.,* **59**: 119–121, 1985.
132. B. Gross, J. Bow, and S. V. Nablo, Charge buildup in electron-irradiated dielectrics, *J. Appl. Phys.,* **44** (6): 2459–2463, 1973.
133. B. Gross, G. M. Sessler, and J. E. West, Charge dynamics for electron-irradiated polymer foil-electrets, *J. Appl. Phys.,* **45** (7): 2841–2851, 1974.
134. M. Falck, G. Dreyfus, and J. Lewiner, Vapor-induced depolarization current. I. Models, *Phys. Rev. B,* **25**: 5499–5508, 1982.
135. N. Falck, G. Dreyfus, and J. Lewiner, Vapor-induced depolarization current. II. Models, *Phys. Rev. B,* **25**: 5509–5514, 1982.
136. M. S. Khalil and B. S. Hansen, Investigation of space charge in low-density polyethylene using a field probe technique, *IEEE Trans. Electr. Insul.,* **23**: 441–445, 1988.
137. C. M. Cooke and C. W. Manglesdorf, Bulk charging of epoxy insulation under stress, *IEEE Int. Symp. Electr. Insul.,* Boston, 1980, pp. 146–149.
138. M. Yashima, H. Fujinami, and T. Takuma, Measurement of accumulated charge on dielectric surfaces with electrostatic probe, in L. Christophorou (ed.), *Gaseous Dielectrics V,* Oxford, UK: Pergamon Press, 1987, pp. 242–248.
139. D. K. Davies, The examination of electrical properties of insulators by surface charge measurements, *J. Sci. Instrum.,* **44**: 521–524, 1967.
140. T. R. Foord, Measurement of the distribution of surface electric charge by the use of capacitive probe, *J. Phys. E,* **2**: 411–413, 1969.
141. H. J. Wintle, Theory of the potential probe used in static electrification measurements on insulators, *J. Phys. E,* **3**: 334–336, 1970.
142. G. M. Sessler and J. E. West, Method for measurements surface charge densities on electrets, *Rev. Sci. Instrum.,* **42**: 15–18, 1971.

D. K. DAS-GUPTA
University of Wales

SPACE-CHARGE-LIMITED CONDUCTION. See CHARGE MEASUREMENT.

SPACECRAFT CONTROL. See ATTITUDE CONTROL.

SPACECRAFT TELEMETRY. See TELEMETRY.

SPACES, HILBERT. See HILBERT SPACES.

SPACE-TIME ADAPTIVE PROCESSING (STAP). See ADAPTIVE RADAR.

SPACE-TIME PROCESSING. See ANTENNA ARRAYS FOR MOBILE COMMUNICATIONS.

S-PARAMETERS, MICROWAVE AMPLIFIER DESIGN. See MICROWAVE AMPLIFIERS.